

Rotorcraft pilot coupling susceptibility accompanying handling qualities prospects in preliminary rotorcraft design.

D. Yilmaz, B. Dang Vu, M. Jones

► **To cite this version:**

D. Yilmaz, B. Dang Vu, M. Jones. Rotorcraft pilot coupling susceptibility accompanying handling qualities prospects in preliminary rotorcraft design.. 39th European Rotorcraft Forum, Sep 2012, MOSCOU, Russia. <hal-01061247>

HAL Id: hal-01061247

<https://hal-onera.archives-ouvertes.fr/hal-01061247>

Submitted on 5 Sep 2014

HAL is a multi-disciplinary open access archive for the deposit and dissemination of scientific research documents, whether they are published or not. The documents may come from teaching and research institutions in France or abroad, or from public or private research centers.

L'archive ouverte pluridisciplinaire **HAL**, est destinée au dépôt et à la diffusion de documents scientifiques de niveau recherche, publiés ou non, émanant des établissements d'enseignement et de recherche français ou étrangers, des laboratoires publics ou privés.

ROTORCRAFT PILOT COUPLING SUSCEPTIBILITY ACCOMPANYING HANDLING QUALITIES PROSPECTS IN PRELIMINARY ROTORCRAFT DESIGN

Deniz Yilmaz
Delft University of Technology, The Netherlands

Binh Dang-Vu
ONERA, France

Michael Jones
University of Liverpool, United Kingdom

Abstract

Due to expensive and risky Rotorcraft-Pilot Couplings (RPC) that can develop during flight testing phases of any new prototype aircraft, it is beneficial to crosscheck the RPC susceptibility of the vehicle as early as possible during the design process. One of the objectives of the European project ARISTOTEL (2010-2013) is to provide guidelines to designers and simulator programs to reveal RPC aspects of the vehicle to be designed. First, a methodology to assess the sensitivity of Handling Qualities (HQs) and RPCs to design parameters is presented: a design envelope is created around a baseline configuration while considering various parameter constraints and simulation models in state space representation are developed. Second, three PIO criteria are applied to predict the susceptibility to PIO of a set of configurations belonging to the design envelope. Assessment based on Bandwidth-Phase Delay (BPD) reveals that the lowest tip speed values and the lowest disc loading values have the best HQs. Category II PIO assessment based on Open Loop Onset Point (OLOP) shows that lowest actuator rate limits are obtained for the configurations with high tip speed values and high disc loading values. PIO prediction based on the newly developed Predictive Phase-Aggression Criterion (PRE-PAC) shows that results for models tested reflect those of the BPD criteria.

1. INTRODUCTION

Parallel to the evolution of sophisticated enhancements in rotorcraft technology and subsystems, flight test programs have been troubled with a persistent safety phenomenon: Pilot Induced Oscillations (PIO's). PIO's, and more general aircraft/rotorcraft pilot couplings (A/RPC's) phenomena have manifested since the first powered flight. Fixed and rotary wing aircraft have been experiencing this safety threatening phenomenon, and various prediction and prevention tools have been developed for them. Recently, the European Commission project ARISTOTEL [1–3] aimed to advance the state of the art of A/RPC. One of the targets of the project is to provide guidelines to designers and simulator programs to reveal A/RPC aspects of the vehicle to be designed or to be evaluated. Due to expensive and risky A/RPC that can develop during flight testing phases of an aircraft development program, it is highly beneficial to crosscheck the A/RPC susceptibility of the vehicle as early as possible during the design process.

During the conceptual design phase the manufacturer has a big freedom to modify the rotorcraft design without strong influences on the costs. The aerodynamics characteristics, actuator performance, or flight control system structure may be modified, since the final configuration has not been frozen at that time. Many design points have to be matched and many disciplines such as aerodynamics, structures, materials, performance and weight analysis, have to be compromised. Generally, Handling Qualities (HQ's) are assessed at a later stage where the rotorcraft and flight control are developed further and models are commonly available for all subsystems. Without being exhaustive, this study aims to unmask effects of some preliminary rotorcraft design parameters on HQ's and RPC's, via a number of analysis criteria. The paper is organised as follow: after a short introduction, Section 2 presents the methodology to assess the sensitivity of HQ's and RPC's to rotorcraft design parameters. The baseline rotorcraft configurations on which variations on the design parameters are applied is the BO105. Section 3 presents the application of traditional and newly developed RPC analysis criteria to the above

configurations: Bandwidth Phase Delay (BPD) [4], Open Loop Onset Point (OLOP) [5], Phase-Aggression Criteria (PAC) [6]. Following, correlations between the results for various design points will be elaborated.

2. METHODOLOGY

2.1. Design envelope creation

A design envelope was first created while considering various parameter constraints. Table 1 shows the parameter boundaries and summary of the descriptions of these constraints [8-13] (as related to the BO105 helicopter). For example, Figur shows the disc loading database configurations of existing helicopters with various gross weights. Estimation fit [7] in Figur was used with $\pm 10\text{kg/m}^2$ interval while designing the available parameter envelope.

Preliminary design parameters such as those listed in Table 1, are comprehensive measures such that they are tailored by basic main rotor properties and helicopter weight. For example, for a rectangular rotor blade design, solidity depends on the rotor radius, number of blades and the chord of the blade. Thus, preliminary design parameters could be considered as a fundamental signature which is formed by independent design parameters such as sizing and weight.

Table 1. Design parameter envelope boundaries.

Design Parameters	Values	Constraint Descriptions
Aspect Ratio (-)	Min. 14	<i>Aerodynamic performance (high induced drag)</i>
	Max. 20	<i>Structural efficiency</i>
Solidity (-)	Min. 0.06	<i>Hover performance</i>
	Max. 0.12	<i>Manoeuvrability</i>
Tip Speed (ft/s)	Min. 400	<i>Compressibility, noise issues</i>
	Max. 780	<i>Retreating blade stall, autorotation issues</i>
Disc Loading (-)	Min. Figur	<i>Rotor size</i>
	Max. Figur	<i>Autorotation landing capability</i>
Blade Loading Coef. (-)	Min. 0.05	<i>Structural efficiency</i>
	Max. 0.1	<i>Onset of blade stall, increase of vibratory loads</i>

According to Table 1, a multi-dimensional design space can be defined with available design points within this bounded design envelope. In this study, a subspace of design configuration was selected based on BO105 helicopter specifications to be used as baseline. For example, weight was limited to 'light'

helicopter class (1.5 – 3.5 tones), as shown in Figur.

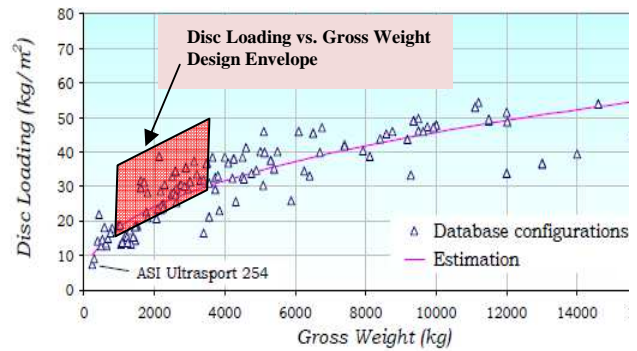


Figure 1: Disc loading design envelope with gross weight, plotted on the database configurations and the estimation of Ref. [7].

Intervals of varied main rotor sizing parameters and gross weight are tabulated in Table 2.

Table 2. Design interval of independent parameters.

Parameters	Min.	Max.
Radius (m)	3	7
Omega (rad/s)	20	80
Weight (kg)	1500	3500
Number blades	3	5

An algorithm was developed to perform the sweep of main rotor parameters and rotorcraft weight within the assigned design interval which is listed in Table 2. After defining the design interval, a calculation loop swept from lower to higher values of each design interval values, while storing the design points which satisfy the boundaries in Table 1. As a result, a subspace of satisfactory design points was obtained within the desired design constraints of Table 1 and Table 2. These envelopes practically guide the designer to elaborate any available design point for any helicopter within this design envelope.

The obtained design envelopes are shown in Appendix, Figures A.1 to A.3. Five design points for each number of blade configurations were selected, as shown in Figures A.1 to A.3. Considering the solidity variation maps, five design points were chosen in order to represent the peaks of each parameter map, see Figures A.1 to A.3. Table A.1 provides the values of the chosen design parameters.

2.2. Simulation model development

Figure 1 summarizes this procedure to obtain the frequency domain design model with varied preliminary design parameters. First, chosen design points were input to the simulation framework, step 1 in Figure 1.

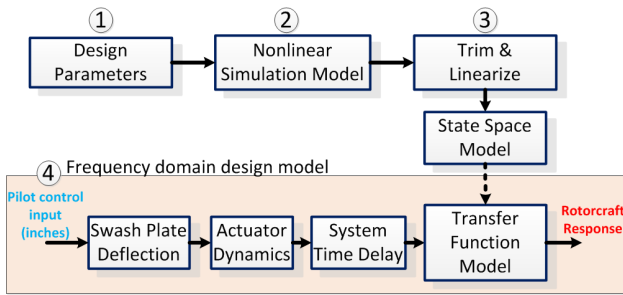


Figure 1: Flow chart of obtaining frequency domain rotorcraft models with varied design parameters.

As for step 2 in Figure 1, a non-linear BO105 simulation model was applied within ARISTOTEL project [1–3] after being validated against flight test data. This model was utilized by variable design parameter features. Then, this model was trimmed and linearized (as shown step 3 in Figure 1) and the resultant linearized 18 degree of model (body, rotor flap, lead-lag, inflow, and tail rotor states) were reduced to 8 degree of freedom (body states with coupled quasi-linear rotor states) models with adjustable design parameter options.

During the variation of design parameters such as those listed in Table 2, physical dimensions of BO105 (except the rotor) were kept constant. Body inertias are scaled with respect to corresponding design weight. It was assumed that flight control system was able to provide the required trim control input for any design configuration.

According to ADS-33, velocities up to 45 knots are considered as low speed and higher velocities are categorized as forward speed [14]. Hence, linearized simulation models were obtained for hover, 30 and 60 knots, in order to cover fundamental velocity regimes. Then, linearized models were used to obtain state space model matrices, namely stability matrix A and control matrix B. This state space representation of the system inherently provides aerodynamic damping values in body axes. Moreover, transfer functions of this state space models were obtained in order to be used in frequency domain criteria analysis, as shown step 4 in Figure 1.

First order low pass filter structure was used to model the actuator dynamics, with a time constant of 0.04s [1]. During the transfer function model extraction of the simulation model, 200ms time delay was added to the whole helicopter system, in order to present a regular system delay in helicopters [15]. Finally, step 4 in Figure 1 shows the block diagram of comprehensive frequency domain simulation model which includes aspects that were listed above.

In order to compare trim control inputs and Euler angles of all design configurations, Figure B.1 is plotted with all chosen design point trim values. It was observed from Figure B.1 that trim values were

close enough to assume the full functionality of the flight control system for all configurations.

At this final stage, time and frequency domain representations of designed rotorcraft configurations were obtained to be used in RPC analysis methods, which will be discussed in following sections.

3. APPLICATION OF RPC ANALYSIS CRITERIA

3.1. Bandwidth-Phase Delay

In ADS-33 [14], bandwidth phase delay (BPD) criterion was introduced for rotorcraft handling quality assessment for hover, low speed and forward flight phases. Although the origin of the criterion belongs to fixed wing research, BPD showed its value in rotorcraft handling and flying qualities assessments as well. From RPC perspective, unlike the fixed wing applications, rotorcraft BPD criteria do not have defined PIO boundaries yet. However, for Attitude Command Attitude Hold (ACAH) rotorcraft control systems, a warning is included about RPC-proneness of the vehicle depending on gain and phase margins, ω_{BWgain} and $\omega_{BWphase}$ respectively [14]. Figure 2 shows the Bodé plot of the vehicle response and corresponding BPD criteria terms.

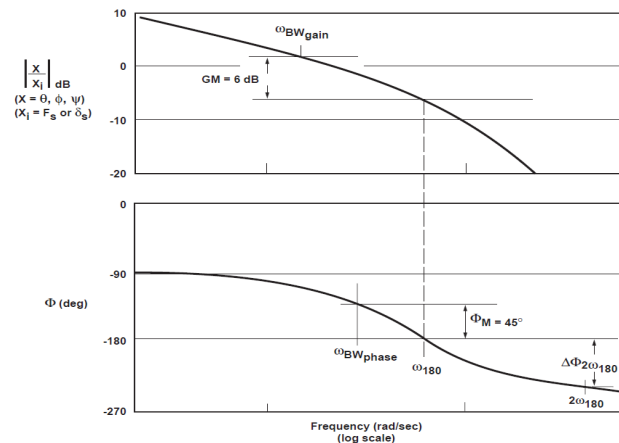


Figure 2: Bodé diagram of BPD determination in ADS-33 [14].

In Figure 2, neutral stability of the system is defined as ω_{180} and the quickness of the higher frequency phase drop is determined by the $2\omega_{180}$ and the phase delay at that frequency. Final phase delay value is calculated by the ratio of this phase drop to the frequency of the drop, as shown in Equation (1).

$$\tau_p = \frac{\Delta\Phi_{2\omega_{180}}}{57.3 (2\omega_{180})} \quad (1)$$

The bandwidth value depends on the command systems, such that Rate Command (RS) systems use the lowest of ω_{BWgain} and $\omega_{BWphase}$, whereas Attitude Command (AC) systems use $\omega_{BWphase}$.

Finally, BPD is plotted on ADS-33 charts with boundaries, as illustrated in Figure 3.

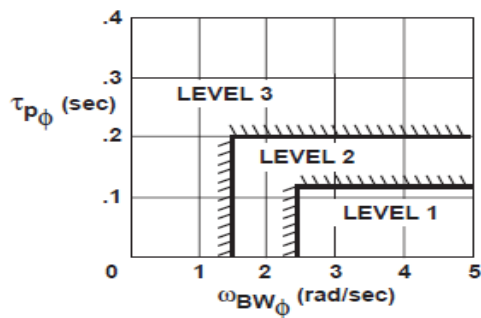


Figure 3: Roll axis BPD HQ boundaries for target tracking and acquisition task during forward flight [14].

In principle, BPD is a pure gain pilot model assessment with closed-loop pilot crossover model of McRuer [16] with the controlled element being the rotorcraft model. Bandwidth represents the maximum closed-loop frequency that the gain pilot model can achieve on the border of system stability [4]. Bandwidth part of the criteria describes the frequency at which the amount of effective pilot control is assessed within system neutral stability. Phase delay part of the criteria is mainly related to the equivalent time delay of the system, such that it describes how fast the phase drops after the neutral stability of the system. The link between BPD HQ and RPC susceptibility generally shows itself in high demands of pilot lead compensation, which is due to large phase delays and low bandwidth values of the vehicle response, particularly around crossover frequency and high gain flying tasks.

The above described configurations, and their transfer function representations were used to calculate BPD of each configuration per axis. Pitch and roll axes are considered in this study, since varied preliminary design parameters were primarily effective on longitudinal and lateral response of the rotorcraft. Determinations of bandwidth of each design configuration are shown in Figure C.1 in the Appendix. It is clear from the figure that selected design configurations are phase limited such that lowest bandwidths are phase bandwidth values. Apart from the design configuration, one of the reasons for this could be the additional system time delay, which drops the phase at high frequencies for a first order rate command system.

Finally, longitudinal and lateral axes BPDs of design configurations are depicted in Figure C.2 and Figure C.3, longitudinal and lateral axis respectively. It can be seen from Figure C.2 and Figure C.3 that configuration C-XV has the best HQ and C-VI has the poorest HQ, according to BPD assessment of all configurations. In order to investigate the HQ and PIO sensitivity in more details, the configurations were chosen having the number of blades according

to the best and poorer HQ. Configurations C-IV, C-IX and C-XV correspond to good HQ, while C-III, C-VI and C-XI have poor HQ. Figure D.1 and Figure D.2 depict design parameter distributions of all configurations with additional emphasize on these selected design configurations with different BPD results.

Preliminary design parameters

Comparisons of preliminary design parameters, which are listed in Table 1, are shown in Figure D.1.

Aspect Ratio (AR) comparison (see Figure D.1(a)) shows that the majority of the configurations are around low boundary of design space. All configurations with good HQ are also close to the low AR boundary. However, C-VI with the poorest HQ configuration is also in the same AR region. Besides, two other poor HQ configurations have the highest AR values. These comparisons indicate that low AR values do not necessarily assure a good HQ, although all good HQ configurations belong to low AR regime.

Solidity comparison (see Figure D.1(b)) poses that there is higher scatter than AR values, such that a pattern for good or poor HQ could not be concluded. Besides, it must be considered that the selection of all design configuration points in design envelope maps was performed according to their location on solidity maps, which already inherently indicates a spread in configuration values. However, this does not change the fact that there is no conclusive trend among configurations with different HQs.

Disc loading comparison (see Figure D.1(c)) shows that configurations form up a scattered pattern of disc loading values. There is a noticeable pattern for good HQ configurations: the lowest disc loading values have the best HQs. A similar pattern is not observed for the bad HQ configurations, although for configurations with three and four number of blades, poor HQ configurations have the highest disc loading values.

Blade loading coefficient comparison (see Figure D.1(d)) shows a similar pattern as AR, such that majority of the values lie within a certain regime, which is the highest blade loading coefficient boundary of the envelope. However, some clear distinctive low values belong to good HQ configurations. On the other hand, bad HQ regimes are not with the highest peaks of values. The trend of the blade loading coefficient distribution does not provide a conclusive result, but low values show a high tendency to have better HQs.

Tip speed comparison (see Figure D.1(d)) indicates that good HQ configurations have the lowest tip speed values. Moreover, for three and four number of blades configurations, poor HQ configurations belong to highest tip speed values. Besides, for five number of blades configuration, poor HQ is not

necessarily with the highest tip speed value.

Independent design parameters

Comparisons of independent design parameters, which are listed in Table 2, are shown in Figure D.2.

Blade chord and radius distributions (Figure D.2(a) and (b) respectively) show that configurations have scattered values. Design configurations with good and poor HQ values with respect to the BPD criterion also do not clearly belong to any regime of distributions. However, when compared to each other, good BPD HQ configurations have higher blade chord and radius values than the poor HQ configurations. However, Figure D.2(a) and (b) do not assure that high values are always with good HQ or vice versa.

Akin to other independent design parameter trends, weight and main rotor rotational speed parameters do not show a certain trend for good or poor BPD HQ points, see Figure D.2(c) and (d). However, when compared within the HQ group, good BPD HQ configurations have lower weight and rotor rotational speed values than the poor HQ configurations.

Summary of BPD results in the design space

Before summarizing the results, it must be kept in mind that selected configurations belong to distinctive layers of solidity maps per preliminary design parameter. Due to computational expense, this study is limited to these selected configurations. However, summary of remarks on good HQ can be listed in Table 3.

Table 3. Summary of BPD based HQ assessment of various design parameters.

	Design Parameters	BPD HQ tendency
Preliminary	Aspect Ratio	Improved BPD HQ with low AR values
	Solidity	Not a conclusive trend
	Tip Speed	The lowest tip speed values have the best BPD HQs
	Disc Loading	The lowest disc loading values have the best HQs
	Blade Loading Coefficient	Good HQ with low blade loading coefficient values
Independent	Radius	Good HQ with high radius values
	Chord	Good HQ with high chord values
	Weight	Good HQ with low weight values

Main rotor speed	Good HQ with low main rotor speed values
------------------	--

3.2. Open-Loop Onset Point

To aid in the prediction of Category II PIO, a method was developed by DLR using describing function techniques and stability regions on the Nichols chart on a number of existing rate saturated aircraft systems [5]. The Open Loop Onset Point (OLOP) is defined as the frequency response value of the open-loop system at the closed-loop onset frequency. This frequency is the point at which actuator saturation first occurs. The closed-loop system describing function is characterised by a jump phenomenon after rate limiting onset, which can be recognized in a Nichols chart as a significant phase jump (Figure 5). OLOP can be identified as the point where the phase jump starts. If the OLOP is located at high amplitudes the additional phase delay causes an increase in the closed-loop amplitude as demonstrated in the Nichols chart. This increase in closed-loop amplitude provokes stronger rate saturation and, therefore, further increasing phase delay. This mechanism can lead to closed-loop instability. If the OLOP is located clearly below 0 dB, the onset of the rate limiter still causes additional phase delay but the change in closed-loop amplitude is less dramatic.

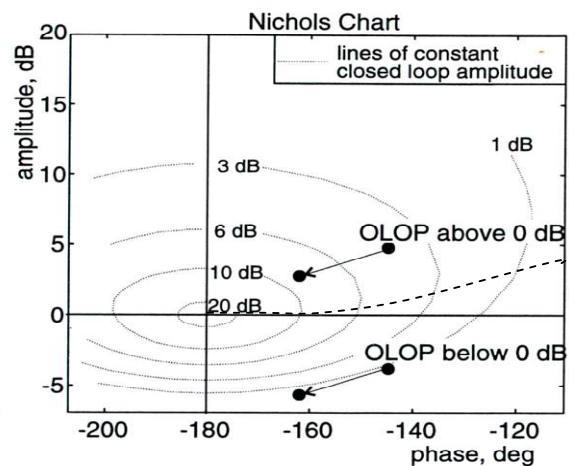


Figure 5: Physical significance of the OLOP parameter.

From off-line analysis of a number of flight experiments a stability boundary was proposed by DLR [5, 17]. As the criterion often over-predicted the susceptibility of certain configurations to PIOs, the modified boundary proposed in Ref. [18] derived from the original one by a 10dB gain shift will be used.

The application of OLOP is dependent on three major factors: pilot model, rate limit, and stick input amplitude. The pilot model affects the general shape

and position of the curve on the Nichols chart. The rate limit and input amplitude affect the position of the OLOP along that curve. In the development of OLOP it was suggested that the pilot be modelled as a pure gain because previous research has shown that a pilot acts as a simple gain during a fully developed PIO (synchronous precognitive behaviour). This gain has to be adjusted based on the linear crossover phase angle of the open-loop pilot-plus-aircraft system. Initially, the authors of OLOP suggested a crossover angle spectrum of -110deg (low pilot gain) to -160deg (high pilot gain) to evaluate pilot gain sensitivity. They also recommended to use maximum pilot input amplitude when determining the onset frequencies. Clearly this is a worst case scenario although it is necessary to verify that this will not produce unreasonable results when compared to flight tests [19]. The results from applying OLOP to the set of configurations C-I to C-XV of the design envelope are presented below. The pilot crossover phase angle is chosen equal to -160deg and the pilot amplitude input is 5deg of cyclic control actuator deflection.

The roll axis OLOP at hover flight is shown in Figure 6 for the configurations C-I to C-V. As indicated in Table A.1, these configurations are with $N=4$ number of blades. Configurations C-I to C-IV become PIO prone as the actuator rate limit is reduced to a value around 6deg/s . Configuration C-V is borderline with a rate limit around 5deg/s .

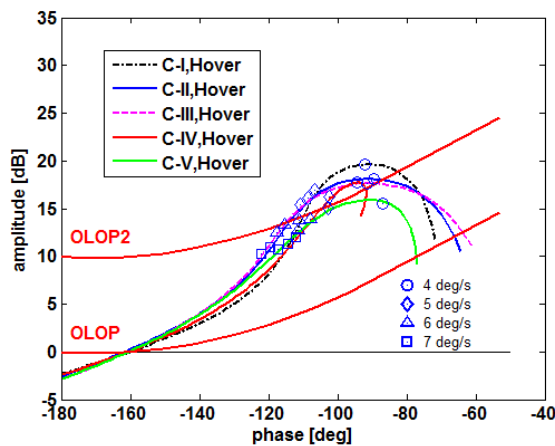


Figure 6: Roll axis OLOP at hover flight

In Table 4, the roll axis OLOP for different velocities shows a noticeable higher rate limit for hover than for 30 knots and 60 knots forward velocities. This suggests that hover is the dimensioning flight condition for determining the minimum rate limit.

Table 4. Roll axis rate limits

	C-I	C-II	C-III	C-IV	C-V
Hover	5.85	5.86	5.67	5.60	4.51
30 kts	2.61	2.01	2.03	3.05	2.02
60 kts	2.58	2.09	2.03	2.15	2.03

The same trend is indeed observed for all the configurations C-I to C-XV. The configuration for which the difference in rate limits between hover and forward flight is the least is C-XV. This can be seen in Figure 7 where each configuration is characterized by a minimum rate limit and an onset frequency. For clarity purposes only the configurations C-XI to C-XV are represented ($N=5$ number of blades).

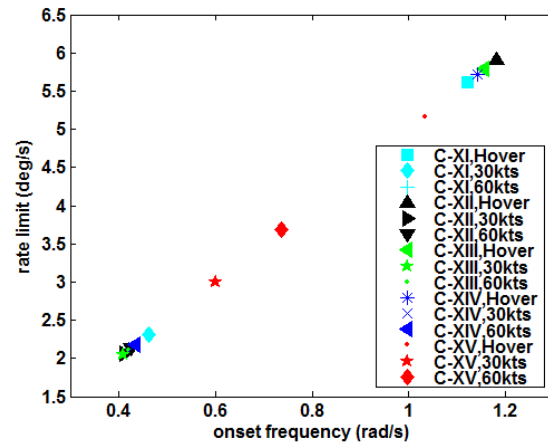


Figure 7: OLOP distribution of configurations with $N=5$ number of blades in roll axis.

Among all the configurations, C-IX has the highest rate limit while C-VI has the lowest (Figure 8), although the differences are relatively small. Thus, lowest minimum rate limits are obtained for configurations with high tip speed values and high disc loading values.

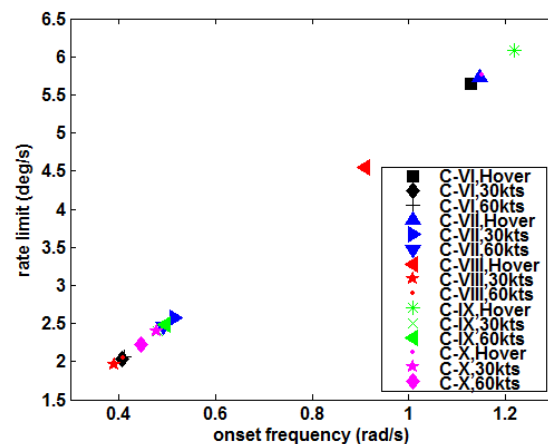


Figure 8: OLOP distribution of configurations with $N=3$ number of blades in roll axis.

For all the configurations it can be checked that the ratio of the rate limit to the onset frequency remains constant and equal to the actuator maximum deflection, i.e. 5deg .

The pitch axis OLOP at 60kts forward flight is shown in Figure 9 for the configurations C-I to C-V. Configurations become PIO prone when the actuator rate limit is reduced to a value around 4.5deg/s . The

configuration C-IV has the highest rate limit, but the difference between the configurations are relatively small as shown in Table 5.

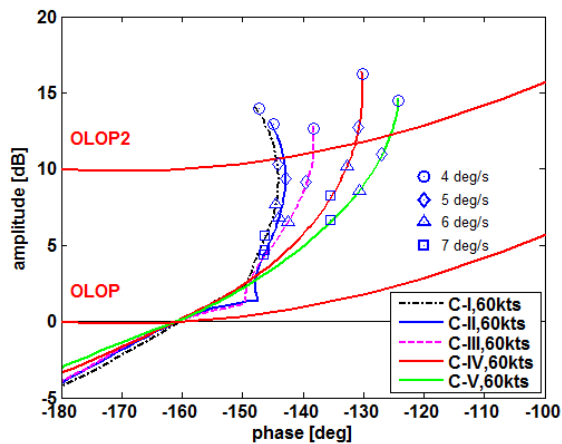


Figure 9: Pitch axis OLOP at 60kts forward flight.

The difference of rate limits between hover flight and forward flight is less important for the pitch axis than for the roll axis as shown in Table 5. The same trend is observed for all the configurations C-I to C-XV.

Table 5. Pitch axis rate limits

	C-I	C-II	C-III	C-IV	C-V
Hover	5.55	4.75	4.10	5.03	4.30
30 kts	4.37	4.20	4.04	4.75	4.39
60 kts	4.87	4.57	4.39	5.37	4.60

Among all the configurations, C-IX has the highest rate limit while C-VI has the lowest (Figure 10). Thus, lowest minimum rate limits are obtained for configurations with high tip speed values and high disc loading values.

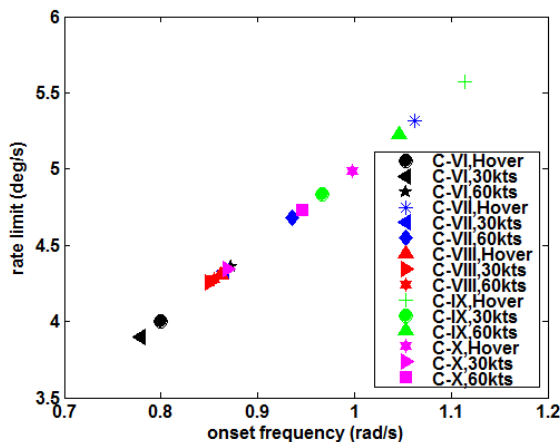


Figure 10: OLOP distribution of configurations with N=3 number of blades in pitch axis.

Summary of OLOP results in the design space

Category II PIO assessment based on OLOP shows that in the roll axis, hover is the dimensioning flight condition for determining the minimum rate limit. In the pitch axis, the difference of rate limits between hover and forward flight is less important. Lowest minimum rate limits are obtained for configurations with high tip speed values and high disc loading values. After the conclusion of the previous section, these configurations produce the worst BPD HQs due to low bandwidth. Low bandwidth configurations yield low crossover frequencies (for the same pilot gain), and low OLOP onset frequencies. As the minimum rate limit is proportional to the onset frequency, the conclusion on the configurations via the OLOP analysis is coherent with the BPD analysis. In the design process a compromise has to be found between good BPD HQ's and low rate limits.

3.3. PRE-Phase Aggression Criterion

This section gives a short description of the criterion, a presentation of the results of C-I to C-V, and their analysis.

The Predictive Phase Aggression Criterion (PRE-PAC) was developed from the real-time capable detection algorithm, the Phase-Aggression Criterion (PAC). The development of PAC is outlined in Ref. [6]. This development effort was initiated to address perceived limitations suffered by existing real-time detection methods. The criterion was developed through the extension of the Pilot-Inceptor Workload (PIW) criteria proposed by Gray [20, 21]. The Phase-Aggression Criterion was adapted through the extension of data sampling to include the dynamics of the vehicle and through the modification to 'real-time' sampling of data throughout the flight manoeuvre. As the name PAC suggests, the information selected to provide an appraisal of the vehicles proximity to a PIO event was the phase difference between pilot input and vehicle output. As the pilot is ultimately interested in achieving a desired attitude, a phase difference of 90° between the attitude rate and inceptor input describes an out-of-phase response (i.e. the attitude lags pilot control by 180°). This is classically one of the most important defining factors required for a PIO to exist.

Throughout the experience of using PAC, it became apparent that it can not only be used as a real-time detection tool, but also used as a prediction tool. This is predictive in the sense that a 'pilot-in-the-loop' is not required. Creating the prediction tool, to complement the detection tool, will hopefully increase both the consistency and synergy between PIO 'prediction' and 'detection'. A full description of the PRE-PAC method, and its method of application, is contained within Ref. [22]. The method is described

briefly in the steps below;

- **STEP1: Define (Simulation) Model:** The initial step in the process requires the user to specify the vehicle model which they wish to use. The complexity of this model is very much dependent on the user requirements. Simplifications of the vehicle model should not be required.
- **STEP 2: Define pilot input signals:** Many prediction tools attempt to unmask PIOs by employing pilot models. PRE-PAC works upon the principle that possible pilot input should be investigated, and not the specific actions of a single pilot. Therefore, sinusoidal input signals, with varying magnitude are defined. These signals should be relative to possible achievable pilot input. It is recommended that to account for system non-linearities, control sweeps are completed at various amplitudes. Figure 11 displays suggested sinusoidal spectrums to be used for the analysis. Here, the frequency dependent amplitude is defined in % of maximum pilot control. These signals represent sinusoids, of steadily increasing frequency and variable magnitude.
- **STEP 3: Calculate Phase and Aggression parameters** from the input and output signals through the computation of the model (defined in STEP 1) with the pilot input signal (defined in STEP 2). These results are recorded for each signal cycle, and can be referenced to input magnitude and frequency.
- **STEP 4: Plot the results** obtained in STEP 3 on the two dimensional phase-aggression chart.

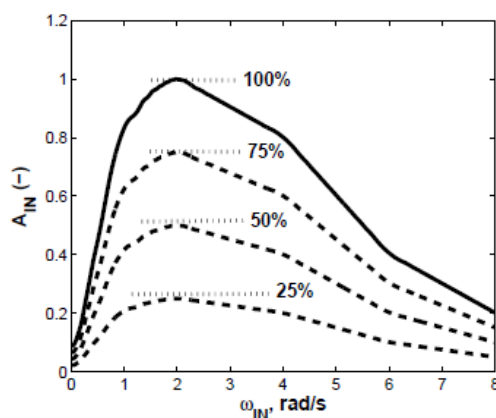


Figure 11: Suggested Input Spectra for PRE-PAC analysis.

Figure 12 displays an example of a result that can be obtained from the use of PRE-PAC. The example shows the results for Case XVI, computed for the 60kt model with the control input signal spectrum 100%, shown in Figure 11. This control signal is intended to be representative of maximum pilot control. The frequency response is computed between 0rad/s and 10rad/s, and at each oscillation new values of phase distortion and aggression are calculated. As shown in Figure 12, it is possible to ascertain the frequency at which the results cross the boundaries. Knowing both the frequency and magnitude of the control input to cause boundary intersection allows one to ascertain the PIO incipient regions of pilot control. In Figure 12, the point where the output signal intersects the Severe PIO region is ascertained as 3.9 rad/s. This denotes that, if the pilot were applying control inputs at 3.9 rad/s, at maximum aggression, they would likely uncover Severe PIO tendencies. The likelihood of the pilot encountering this level of control should be questioned, but this displays that there is the possibility that events will be encountered. This information can be useful in a number of ways. The first is that it allows for the mapping of incipient regions of pilot control. Knowing these regions can allow the designer to either try and mitigate against oscillations or apply procedural limits to ensure that the pilot control does not enter this region. The second use is that simple metrics can be extracted, to provide information regarding the likelihood of PIO. These results can inform in a similar way to traditional bandwidth-phase delay analysis.

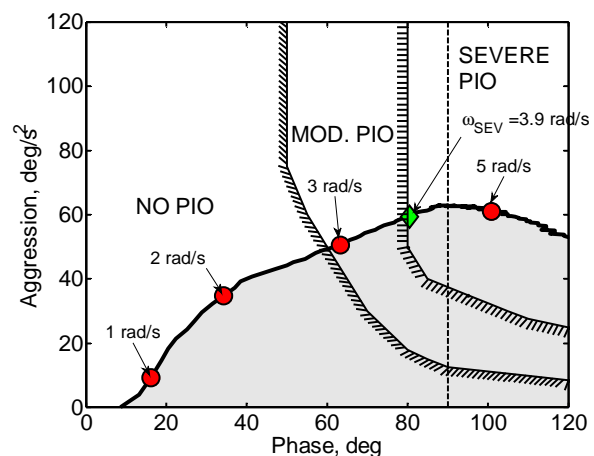


Figure 12: Example of PRE-PAC result.

The PRE-PAC case was used to analyse cases I-V shown earlier in this paper, to judge the RPC sensitivity to design changes. As through results shown in Ref. [22], metrics from the PRE-PAC results can be used to judge incipience to RPC. The two metrics used here were;

- ω_{MOD} = The moderate trigger frequency, whereby the frequency and magnitude of pilot control subsequently causes intersection of the PRE-PAC boundaries.
- $1/(\omega_{SEV}-\omega_{MOD})$ = The inverse change in frequency between the moderate and severe trigger frequencies. Indicates the rapidity of the change in PRE-PAC results following ω_{MOD} .

These two parameters can be used to judge the RPC incipience of each vehicle model. Results for Cases I-V are displayed in Figure 13. These are for the lateral control axis only, for Hover, 30kt, and 60kt flight cases. Here, all results have been computed using boundaries shown in Figure 12. These boundaries have been validated for lateral forward flight manoeuvres. Lower trigger frequency and larger change in frequency indicate stronger tendency for RPC. As the criterion is novel and still under development, the exact contribution to the severity of each parameter is unknown. However, one can use the results here to make some initial conclusions. One such conclusion is that Case III has higher RPC potential than case IV. Another conclusion is that despite comparable moderate trigger frequencies, Case III is likely to cause more catastrophic RPC cases than Case V, due to the larger inverse change in trigger frequency. Comparison to BPD results show strong correlation, with Case 3 having the highest PIO potential.

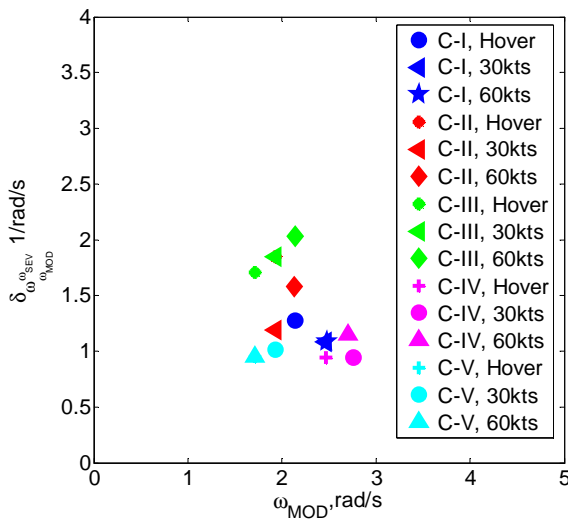


Figure 13: Metrics for N=4 blade models.

Figure 14 shows further examples obtained from computation of roll axis dynamics using PRE-PAC. Here, results are shown for all cases at 30kts. This allows one to see directly the influence of blades within the models. Here one can see of all the cases, Case VI has the strongest RPC incipience. Furthermore, Case XV, has the strongest robustness to RPC. This case has the highest trigger frequency

and lowest inverse change in frequency of all 30 kt cases.

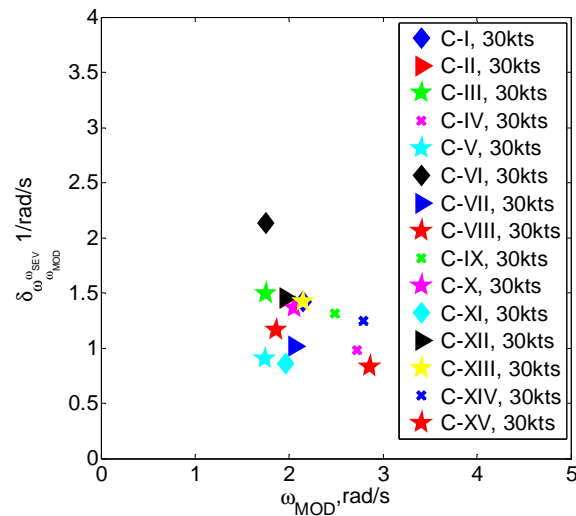


Figure 14: Comparison of 30kt cases.

Cases shown above demonstrate results for maximum pilot control input and ultimately aggression. However, one advantage of PRE-PAC is that it can allow one to see how the potential for oscillations changes with changes in input control magnitude. To demonstrate this change, results from all 60kt cases are shown in Figure 15, for variance control input signals. Results show the progression of metrics as pilot control input signal magnitude (as shown in Figure 11) increases. One can see both the trigger frequency and rate of frequency change is dependent on input signal magnitude. Furthermore, these results can be used to map regions of PIO incipience in pilot control.

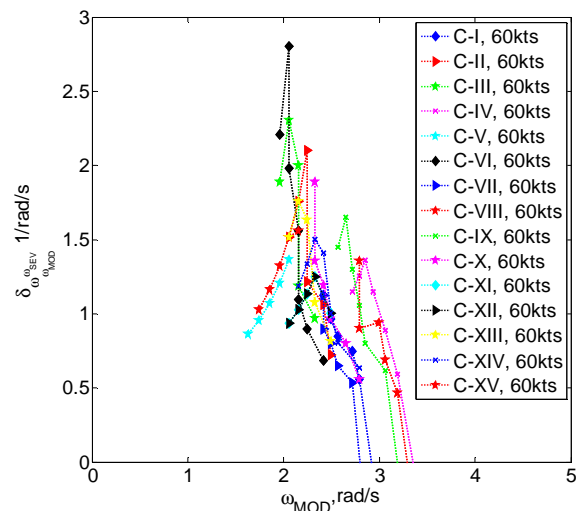


Figure 15: Sensitivity for all models in the study

Overall, although still under development, PRE-PAC results can show an indication of RPC incipience in rotorcraft models. Overall, results for models tested reflect those of the BPD criteria. PRE-PAC offers

further extension to BPD results through the application of non-linear control appraisal, analysis of time variant models, and the evaluation of quasi-linear and non-linear RPC potential.

4. CONCLUSION

The objective of the study was to unmask effects of some preliminary rotorcraft design parameters on HQs and RPCs, via a number of analysis criteria. A design enveloped was first created while considering various parameter constraints and a subspace of design configuration was selected based on BO105 helicopter specifications to be used as baseline. Nonlinear simulation models were developed from the selected configurations and linearized models in state space representation were derived in order to be used in RPC analysis methods. BPD, OLOP and PRE-PAC were applied to predict PIO for the selected configurations.

HQ and Category I PIO assessment based on BPD reveals that the lowest tip speed values and the lowest disc loading values have the best HQs. Good HQs are also predicted for configurations with low aspect ratios and low blade loading coefficients.

Category II PIO assessment based on OLOP shows that in the roll axis, hover is the dimensioning flight condition for determining the minimum rate limit. In the pitch axis, the difference of rate limits between hover and forward flight is less important. Lowest minimum rate limits are obtained for configurations with high tip speed values and high disc loading values.

PIO prediction based on new PRE-PAC criterion shows that results for models tested reflect those of the BPD criteria. PRE-PAC offers further extension to BPD results through the application of non-linear control appraisal, analysis of time variant models, and the evaluation of quasi-linear and non-linear RPC potential.

Acknowledgements

The research leading to these results has received funding from the European Union's Seventh Framework Programme (FP7/2007-2013) under grant agreement No. 266073.

REFERENCES

1. Pavel, M. D., Malecki, J., Dang-Vu, B., Masarati, P., Gennaretti, M., Jump, M., Jones, M., Smaili, H., Ionita, A., Zaicek, L., "Present and Future Trends in Aircraft and Rotorcraft Pilot Couplings — a Retrospective Survey of Recent Research Activities within the European Project ARISTOTEL," 37th European Rotorcraft Forum, Gallarate, Italy, September 13–15 2011, Paper no. 116.
2. Pavel, M. D., Malecki, J., Dang-Vu, B., Masarati, P., Quaranta, G., Gennaretti, M., Jump, M., Smaili, H., Ionita, A., Zaicek, L., "Aircraft and Rotorcraft Pilot Coupling: a survey of recent research activities within the European project ARISTOTEL," 3rd CEAS Air & Space Conference, Venice, Italy, October 24–28 2011.
3. Pavel, M. D., Malecki, J., Dang-Vu, B., Masarati, P., Gennaretti, M., Jump, M., Smaili, H., Ionita, A., Zaicek, L., "A Retrospective Survey of Adverse Rotorcraft Pilot Couplings in European Perspective," American Helicopter Society 68th Annual Forum, Fort Worth, Texas, May 1–3 2012.
4. Mitchell, D.G., Hoh, R.H., Aponso, B.L., Klyde, D.H., "The Measurement and Prediction of Pilot-in-the-Loop Oscillations", AIAA-Paper 94-3670, Scottsdale, 1994.
5. Duda, H., "Effects of Rate Limiting Elements in Flight Control Systems – A New PIO Criterion", AIAA-Paper-95-3304, Aug. 1995.
6. Jones, M., Jump, M., and Lu, L., "Development of the Phase-Aggression Criterion for Rotorcraft-Pilot Coupling Detection", accepted for publication, Journal of Guidance, Control, and Dynamics, AIAA, 2012.
7. Rand, O, Khromov., V., " Helicopter Sizing by StatisticsHelicopter Statistics" , American Helicopter Society 58th Annual Forum, Montreal, Canada, June 11-13, 2002.
8. Milluzzo, J., Leishman G.," Assessment of Rotorcraft Brownout Severity in Terms of Rotor Design Parameters, Journal Of The American Helicopter Society Vol. 55: 032009, 2010.
9. Yilmaz D, Pavel, M.D., Yavrucuk, I, "Helicopter Design For Handling Qualities Enhancement", 35th European Rotorcraft Forum, September 22-25, Hamburg.
10. Prouty, R. W., "Helicopter Performance, Stability, and Control", Krieger Publishing Company, 1995.
11. Leishman, J.G., "Principles of Helicopter Aerodynamics", Cambridge Aerospace Series, 2000.
12. Padfield, D.G., "Helicopter Flight Dynamics: The Theory and Application of Flying Qualities and Simulation Modeling", Published by Blackwell Publishing, 2007.

13. Johnson W., "Helicopter Theory", New York Dover Publications, 1994.
14. Anon., "Handling Qualities Requirements for Military Rotorcraft," Aeronautical Design Standard 33 (ADS-33E-PRF), US Army Aviation and Missile Command, Mar. 2000.
15. M. Tischler, "System Identification Requirements For High-Bandwidth Rotorcraft Flight Control System Design", IEEE American Control Conference, Boston, USA, 26-28 June 1991.
16. McRuer, D., Graham, D., Krendel, E., Reisener, W., "Human Pilot Dynamics in Compensatory Systems", AFFDL-TR 65-15, Wright Paterson AFB, 1965.
17. Duda, H., Hovmark, G. and Forssell, L., "Prediction of Category II Aircraft-Pilot Couplings – New Experimental Results", AIAA-Paper-97-3499, Aug. 1997.
18. Wilmes, T., Duda, H., "Investigation of Electronic Filters to Prevent Aircraft-Pilot-Coupling", Technical Report IB 111-98/29, Institut für Flugmechanik, Braunschweig, Nov. 1998.
19. Gilbreath, G.P., "Prediction of Pilot-Induced Oscillations Due to Actuator Rate Limiting Using the Open-Loop Onset Point Criterion", AFIT/GAE/ENY/01M-02, Air Force Institute of Technology, 2002.
20. Gray, W.R., "Boundary-Avoidance Tracking: A New Pilot Tracking model", AIAA Atmospheric Flight Mechanics Conference, American Institute of Aeronautics and Astronautics Inc., San Francisco, CA, 2005.
21. Gray, W.R., "Handling Qualities Evaluation at the USAF Test Pilot School", AIAA Atmospheric Flight Mechanics Conference, American Institute of Aeronautics and Astronautics Inc., Chicago, IL, 2009.
22. Jones, M., Jump, M., "Prediction of Rotorcraft Pilot-Induced Oscillations using the Phase-Aggression Criterion", Proceedings of the 69th American Helicopter Society Forum, Phoenix, AZ, USA, 2013.

COPYRIGHT STATEMENT

The authors confirm that they, and/or their company or organization, hold copyright on all of the original material included in this paper. The authors also confirm that they have obtained permission, from the copyright holder of any third party material included in this paper, to publish it as part of their paper. The authors confirm that they give permission, or have obtained permission from the copyright holder of this paper, for the publication and distribution of this paper as part of the ERF2013 proceedings or as individual offprints from the proceedings and for inclusion in a freely accessible web-based repository.

APPENDIX

APP.A Design Envelope

Table A.1. Parameter values of design configurations

	I	II	III	IV	V	VI	VII	VIII	IX	X	XI	XII	XIII	XIV	XV
Number of Blades (-)	4	4	4	4	4	3	3	3	3	3	5	5	5	5	5
Radius (m)	7	5	5	6	4	5.2	7	3.9	6.1	5.6	4.8	5.2	5.4	6.8	5.9
Chord (m)	0.45	0.35	0.25	0.4	0.2	0.36	0.48	0.27	0.44	0.39	0.24	0.27	0.38	0.48	0.42
AR (-)	15.56	14.29	20	15	20	14.44	14.58	14.72	14.02	14.36	20	19.26	14.21	14.17	14.22
Solidity (-)	0.0819	0.0891	0.0637	0.0849	0.0637	0.0661	0.0655	0.0649	0.0681	0.0665	0.0796	0.0826	0.112	0.1123	0.1119
Omega (rad/s)	22	38	46	22	50	44	24	52	22	32	36	38	32	20	22
V _{TIP} (m/s)	154	190	230	132	200	229	168	203	134	179	173	198	173	136	130
Weight (kg)	3500	3100	3100	1500	1500	3400	3300	1500	1700	2400	2000	3400	3500	2700	1500
Disc Loading (kg/m ²)	22.74	39.47	39.47	13.26	29.84	40.02	21.44	31.39	14.54	24.36	27.63	40.02	38.21	18.59	13.72
Blade Loading Coef. (-)	0.0938	0.0982	0.0938	0.0718	0.0938	0.0926	0.0929	0.0942	0.0949	0.0913	0.0931	0.0993	0.0915	0.0716	0.0582

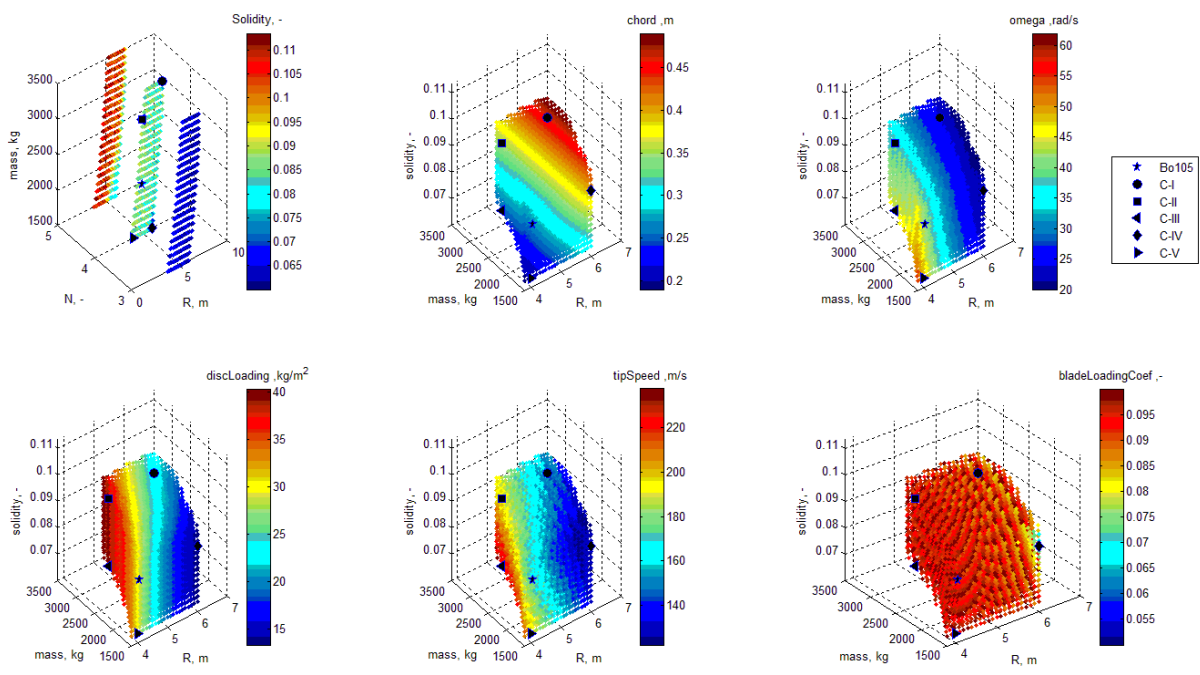


Figure A1: Design envelopes of N=4 blades configurations with five design points and BO105 parameters for reference.

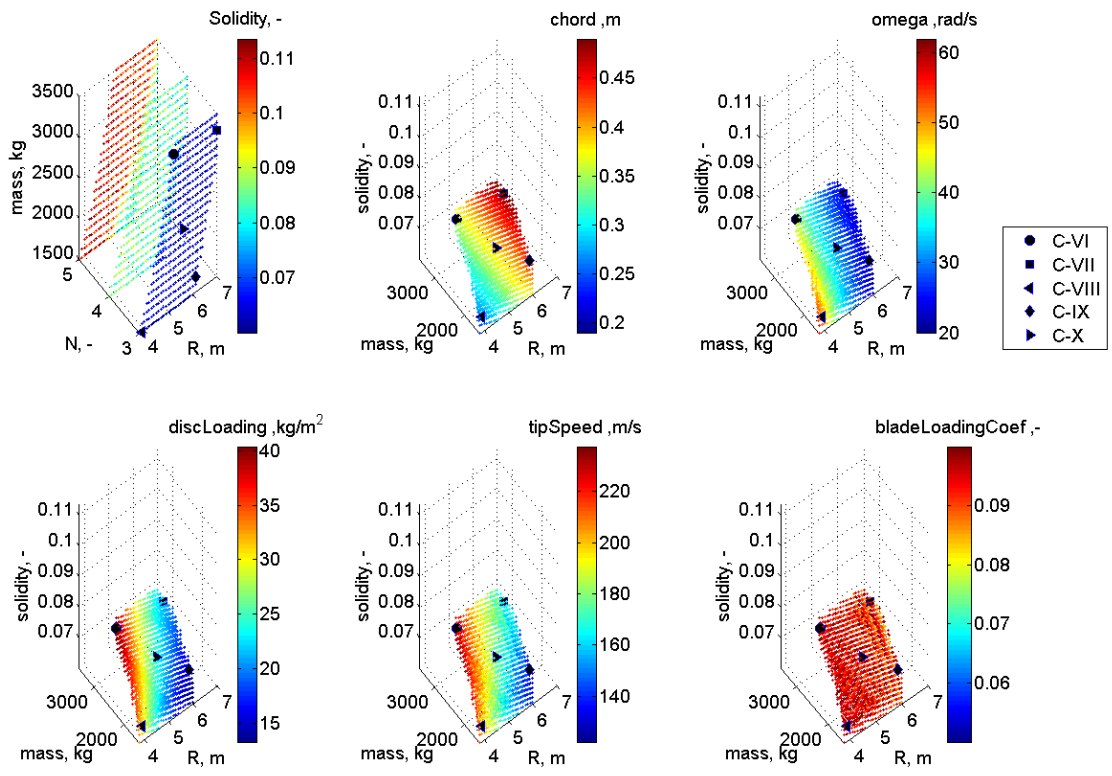


Figure A2: Design envelopes of N=3 blades configurations with five design points.

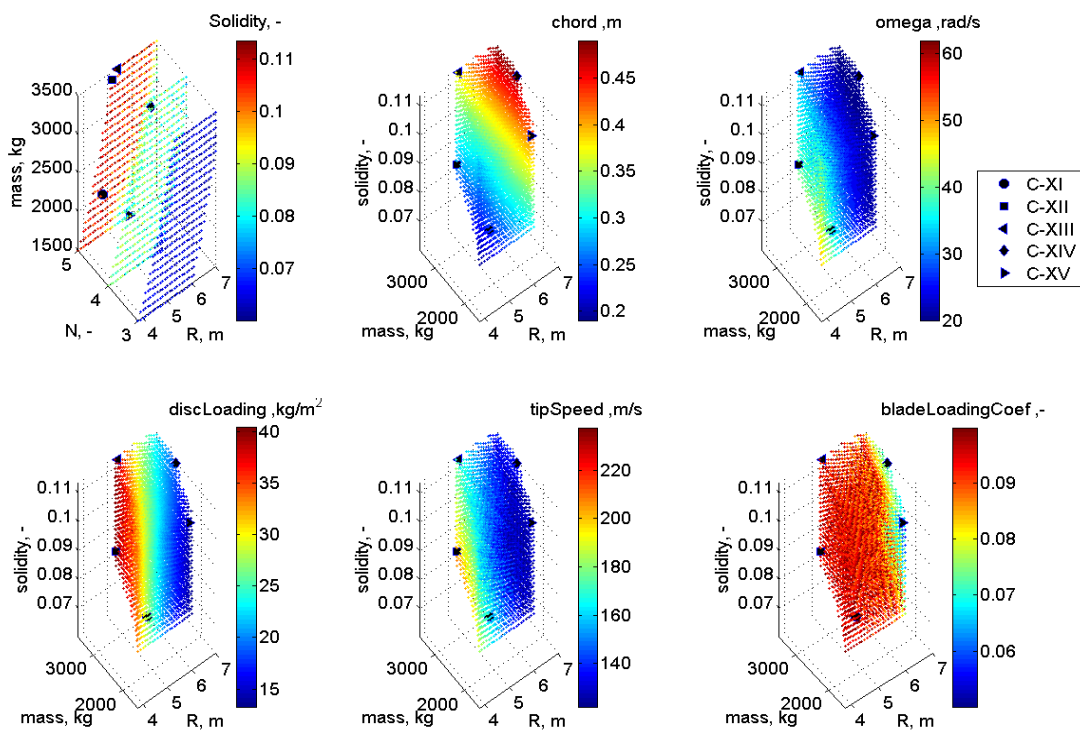


Figure A3: Design envelopes of N=5 blades configurations with five design points

APP.B Trim comparison

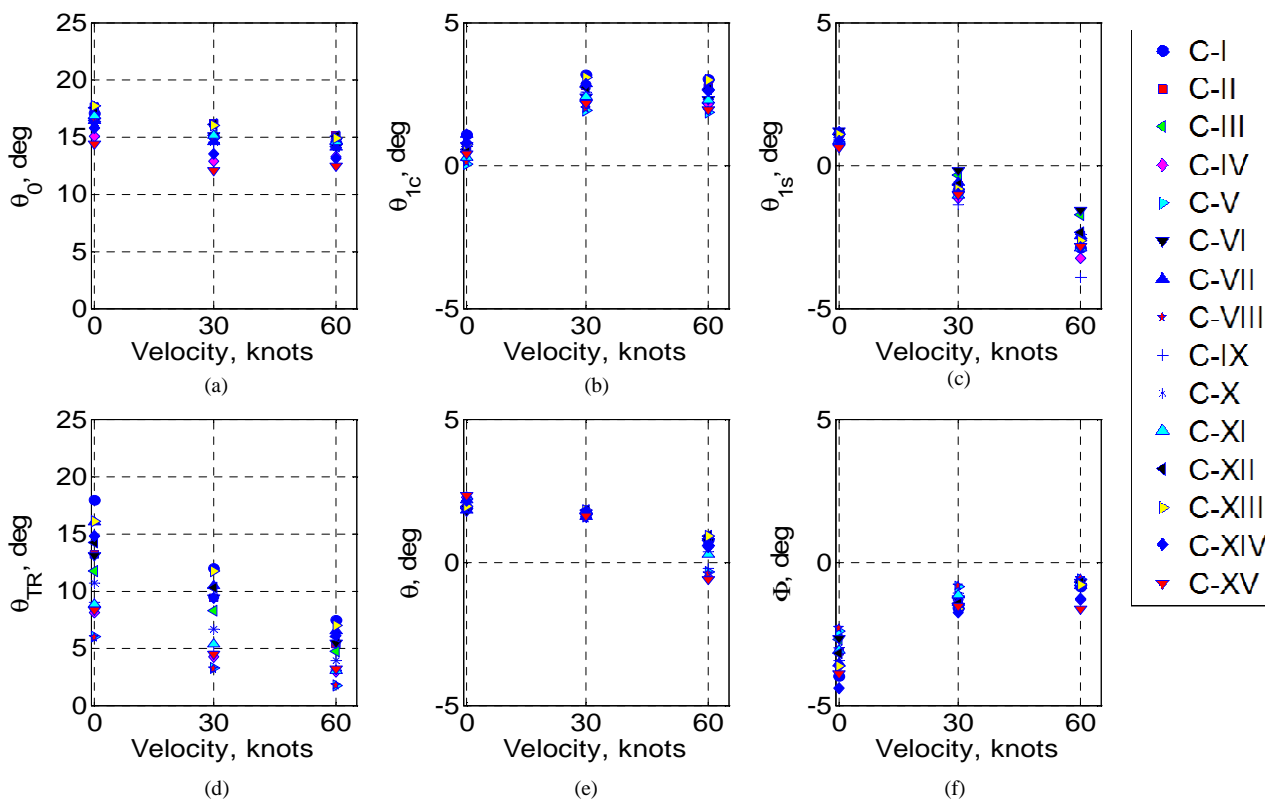


Figure B.1: Design configuration trim values of four control inputs, which are collective (a), lateral (b) and longitudinal (c) swash plates, and pedal inputs (d), and Euler angles for pitch (e) and roll (f).

APP.C BPD assessment

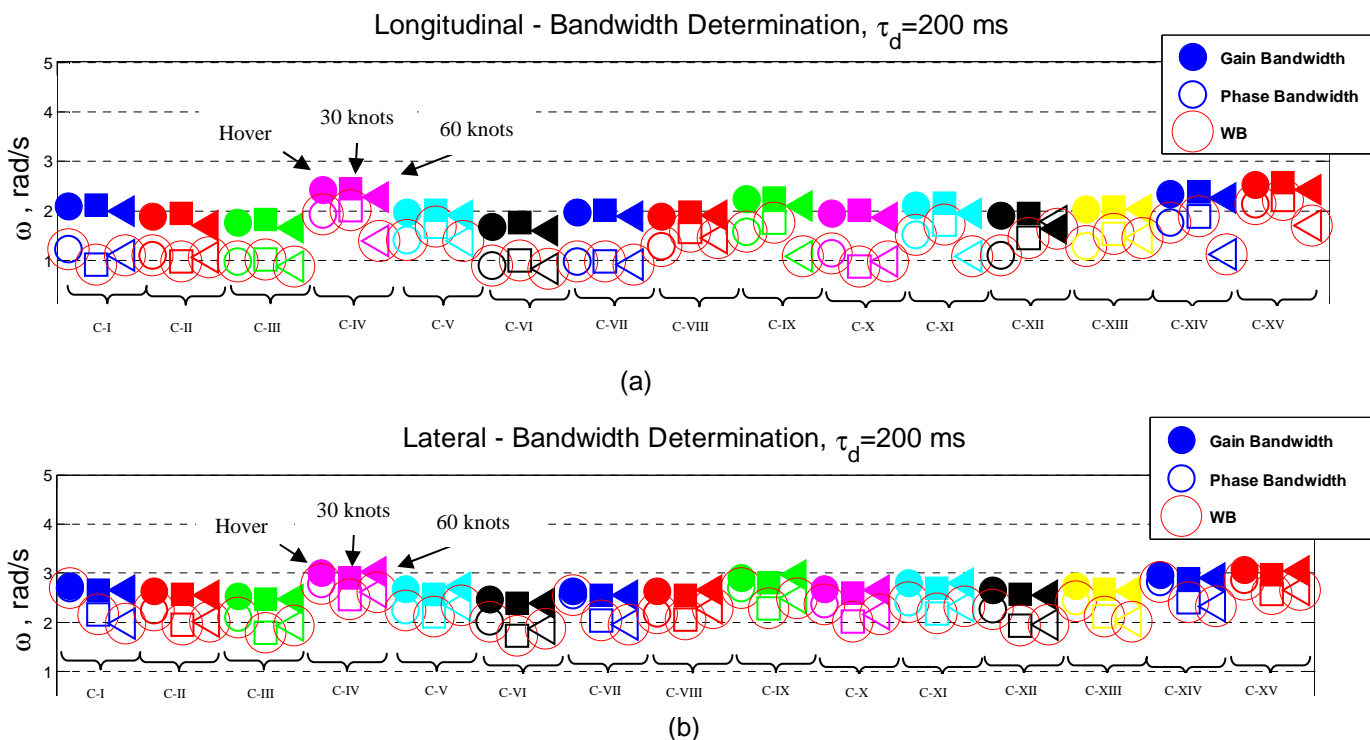
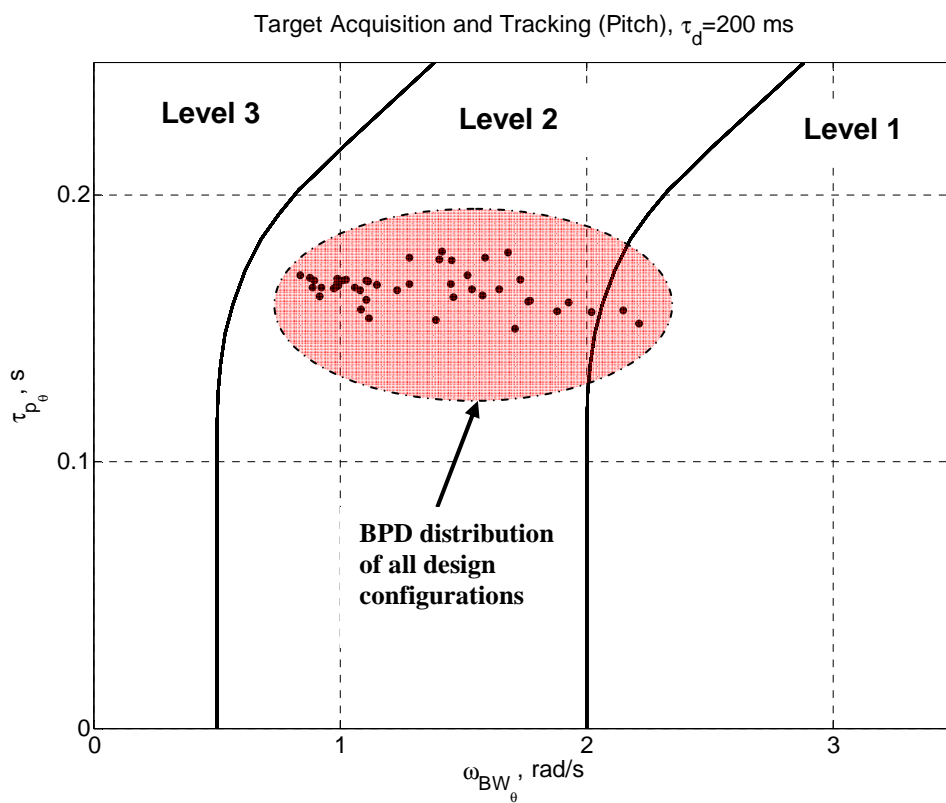
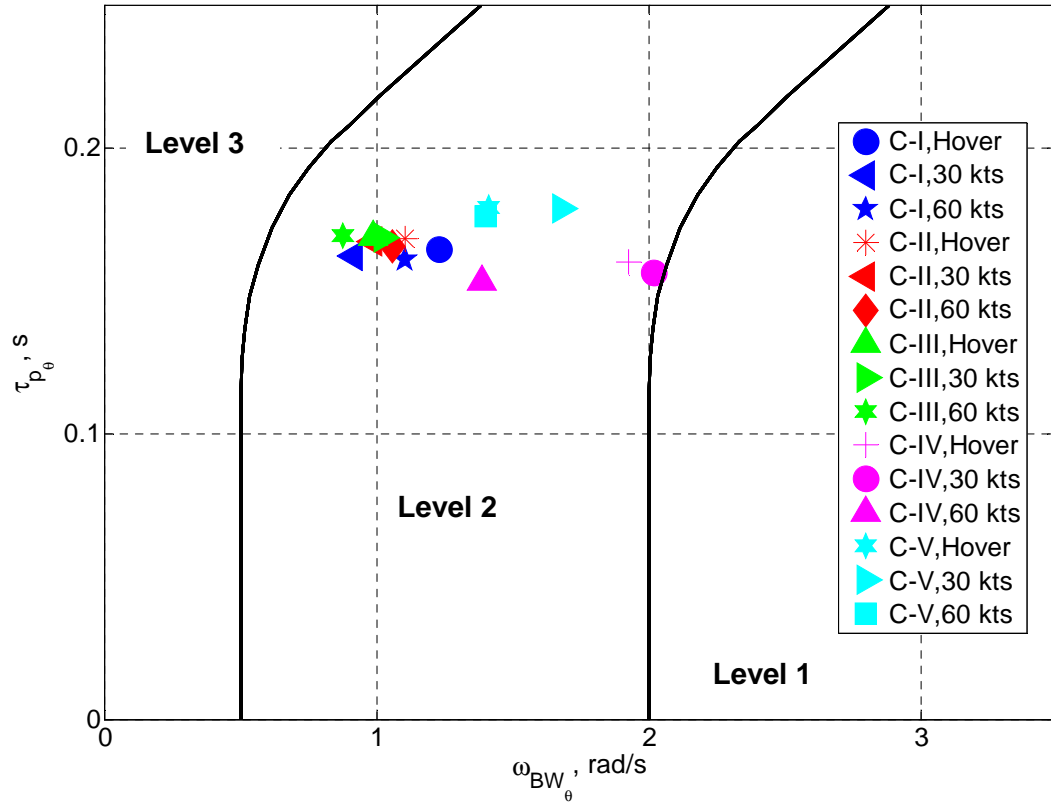
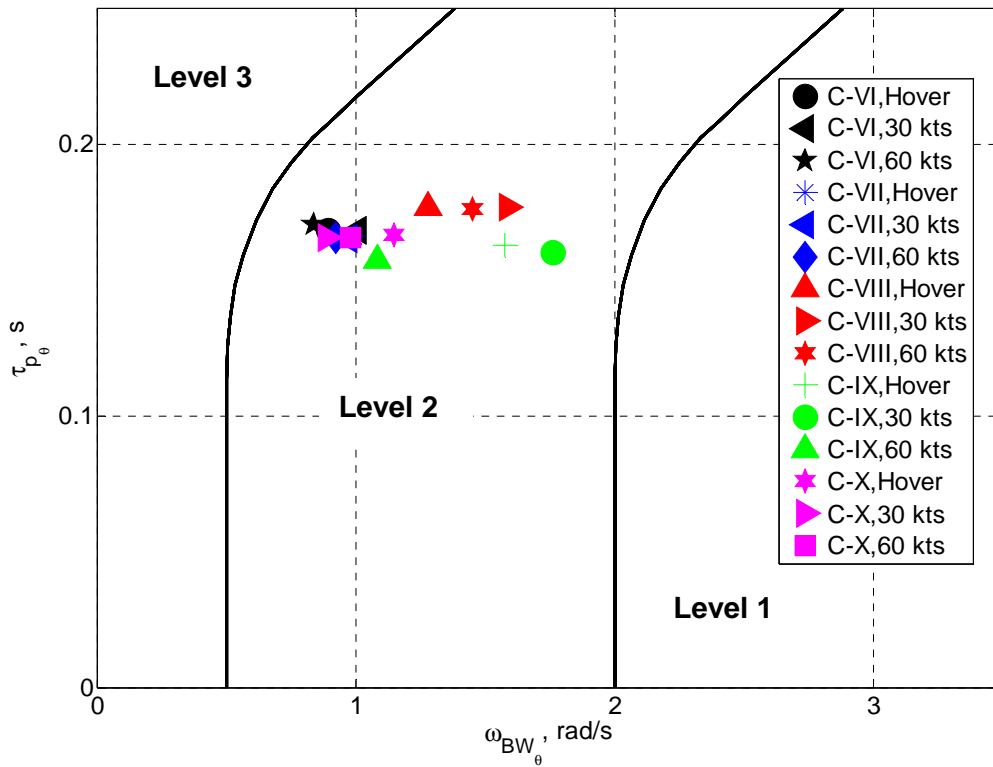


Figure C.1: Longitudinal (a) and lateral (b) bandwidth determination of each design configuration. For each configuration circular, square and triangular markers present hover, 30 knots and 60 knots respectively.

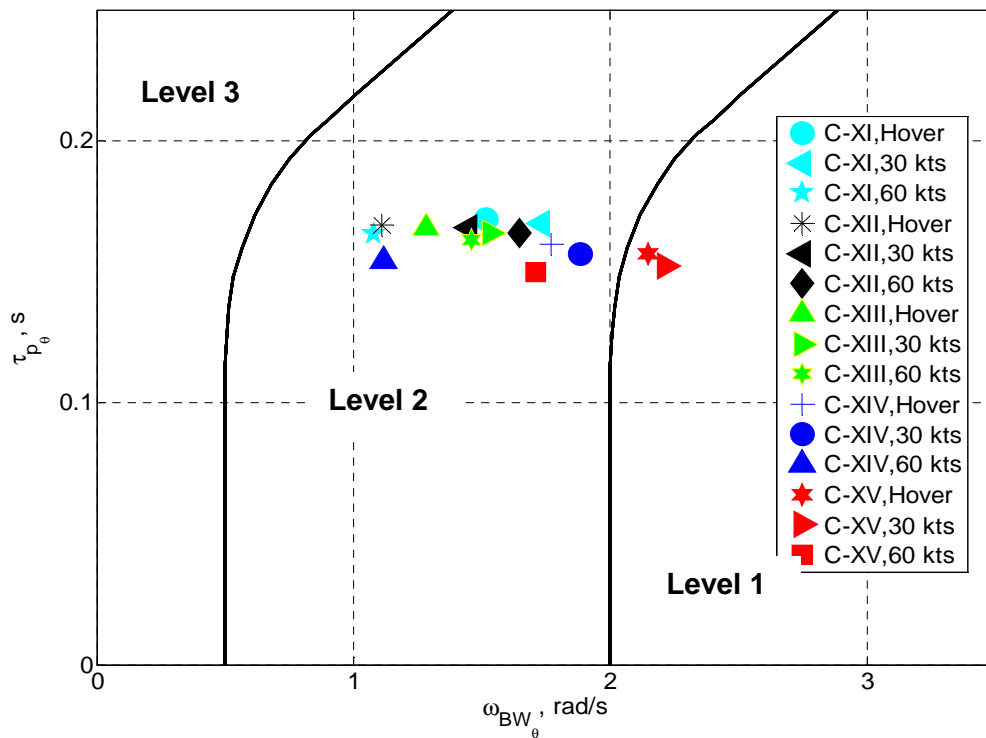




(b) BPD distribution of configurations with N=4 number of blades in pitch axis.

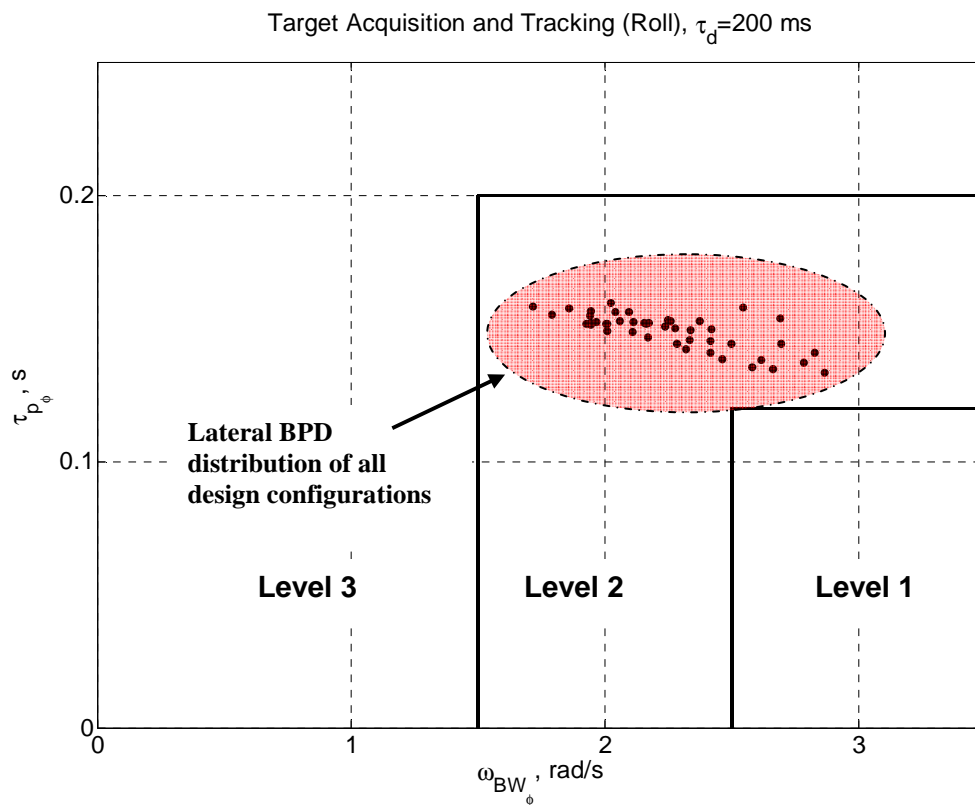


(c) BPD distribution of configurations with N=3 number of blades in pitch axis.

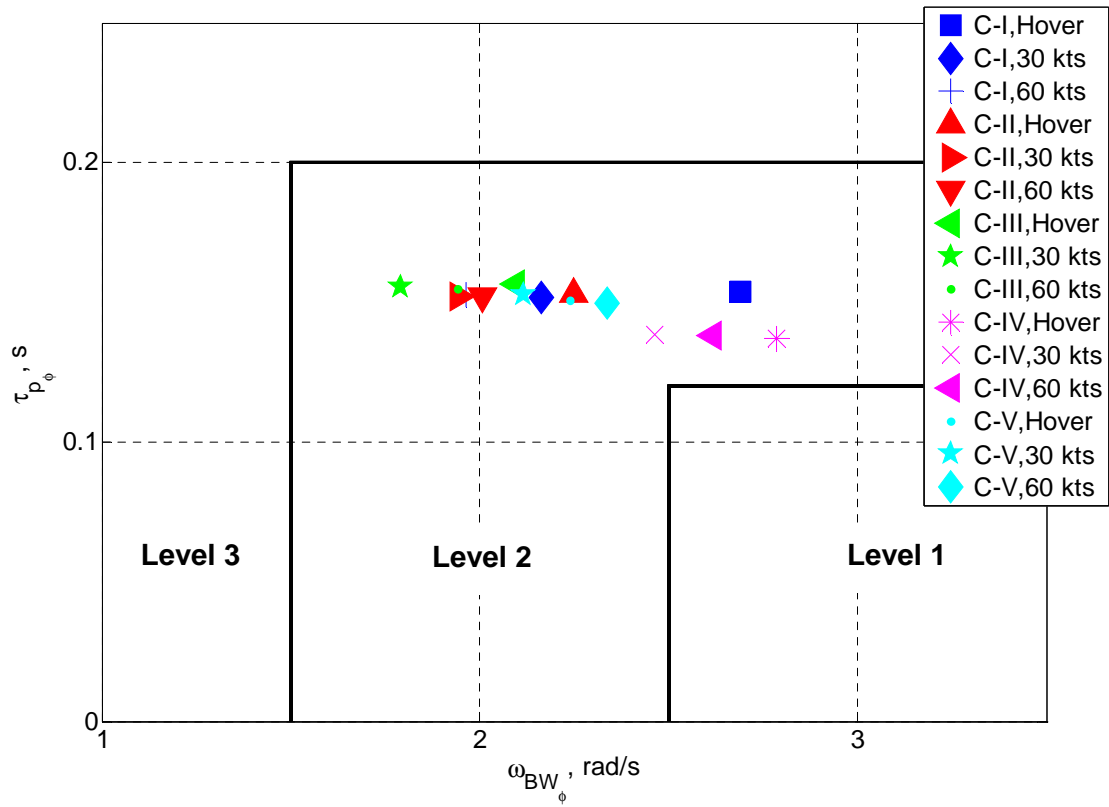


(d) BPD distribution of configurations with N=5 number of blades in pitch axis.

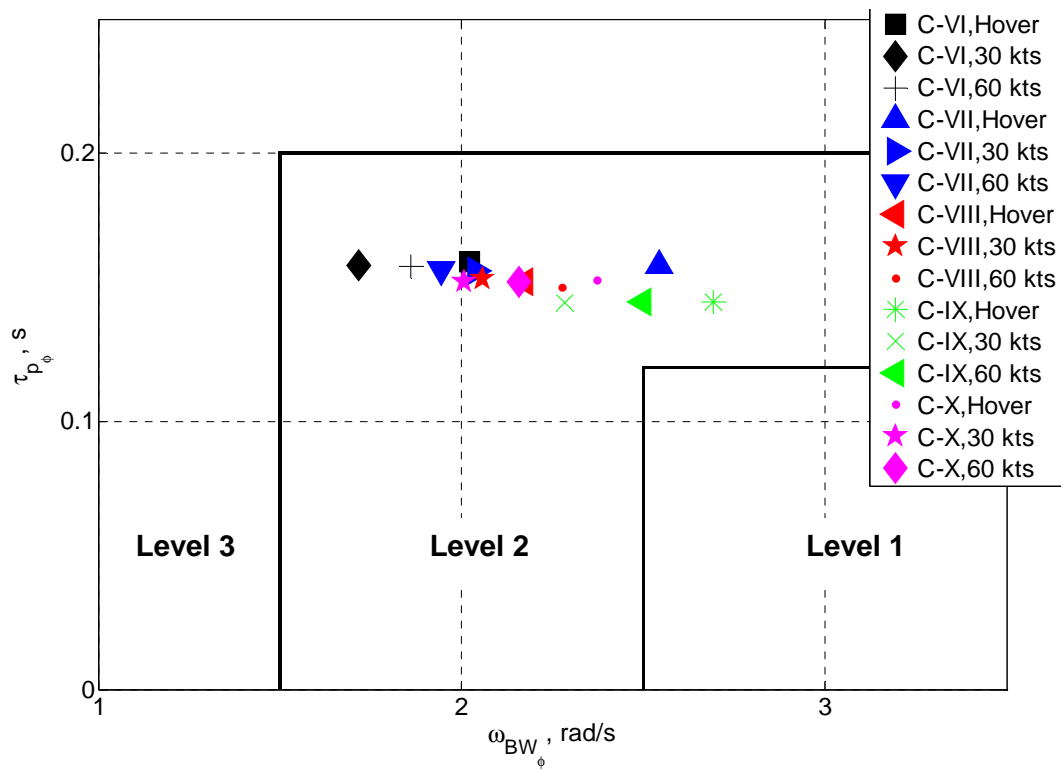
Figure C.2: Longitudinal BPD distribution map of all design configurations (a) and configurations with 4, 3 and 5 number of blades plotted in (b), (c) and (d) respectively



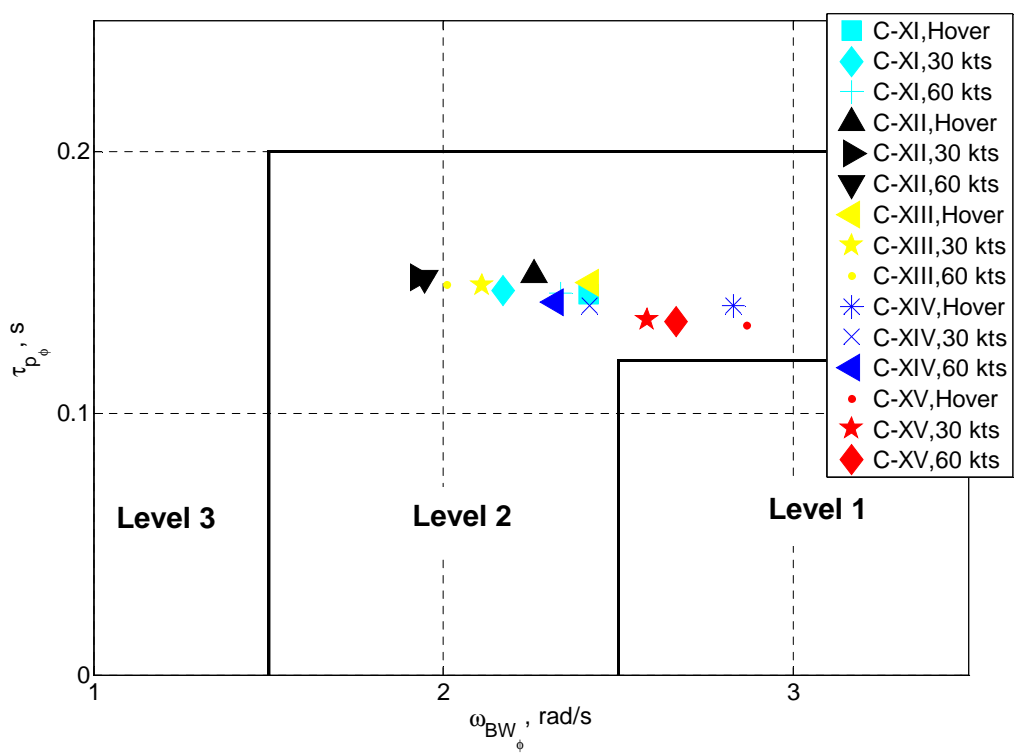
(a) BPD distribution of all design configurations in roll axis.



(b) BPD distribution of configurations with N=4 number of blades in roll axis.



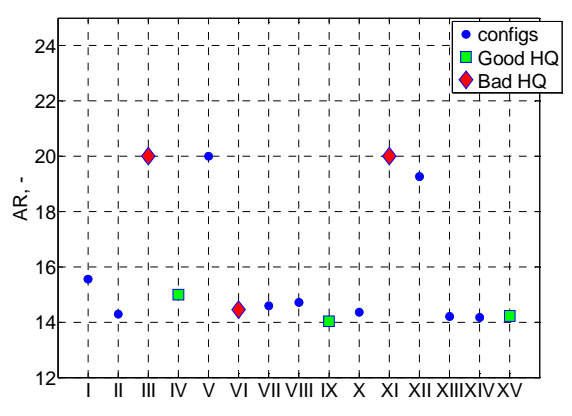
(c) BPD distribution of configurations with N=3 number of blades in roll axis.



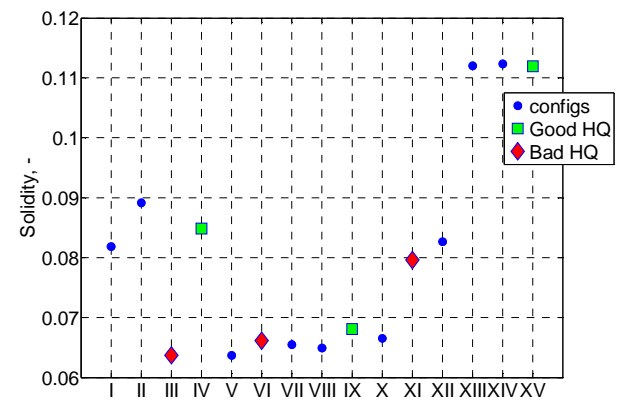
(d) BPD distribution of configurations with N=5 number of blades in roll axis.

Figure C.3: Lateral BPD distribution map of all design configurations (a) and configurations with 4, 3 and 5 number of blades plotted in (b), (c) and (d) respectively

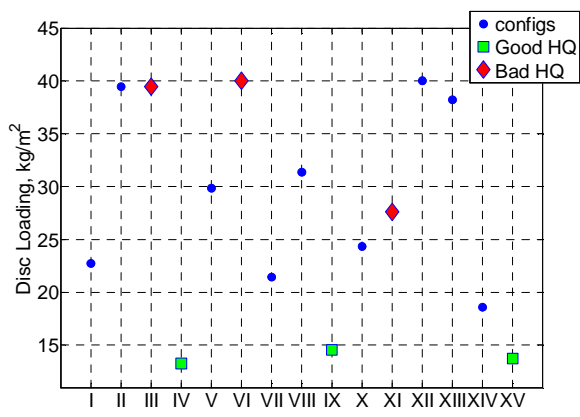
APP.D Design parameter distributions of selected design configurations



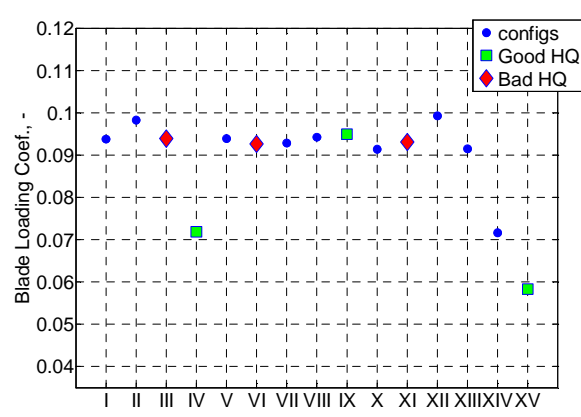
(a) AR comparison



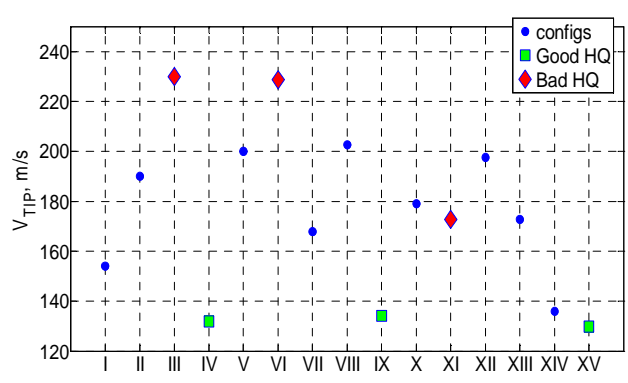
(b) Solidity comparison



(c) Disc loading comparison

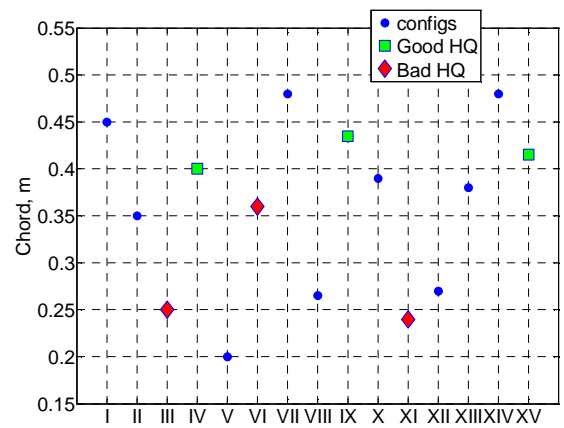


(d) Blade loading coefficient comparison

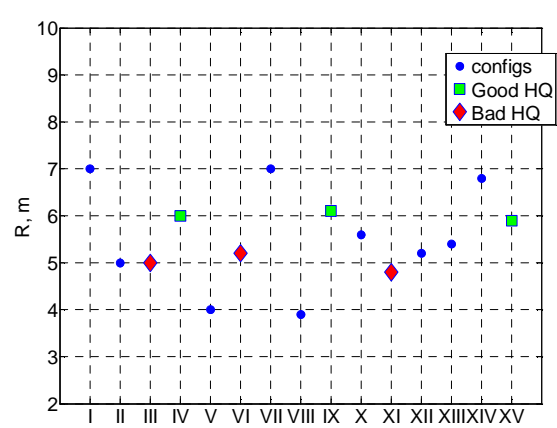


(e) Tip speed comparison

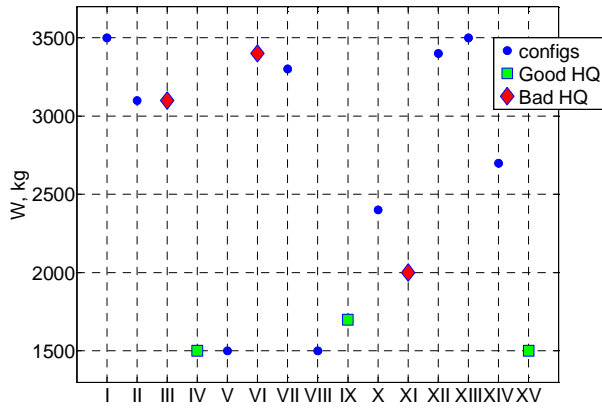
Figure D.1: Preliminary design parameter comparisons among all configurations and the selected ones with good and poor HQs according to BPD analysis.



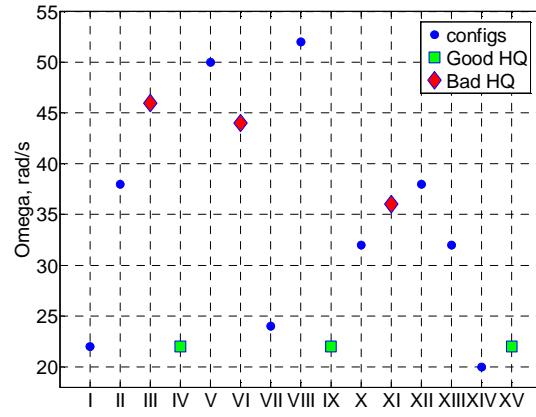
(a) Chord comparison



(b) Radius comparison



(c) Weight comparison



(d) Main rotor rotational speed comparison

Figure D.2: Independent design parameter comparisons among all configurations and the selected ones with good and poor HQs according to BPD analysis.